

Bounds on the recurrence probability in periodically-driven quantum systems

Tanmoy Pandit¹, Alaina M. Green², C. Huerta Alderete², Norbert M. Linke², and Raam Uzdin¹

¹Fritz Haber Research Center for Molecular Dynamics, Hebrew University of Jerusalem, Jerusalem 9190401, Israel

²Joint Quantum Institute and Department of Physics, University of Maryland, College Park, MD 20742 USA

Periodically-driven systems are ubiquitous in science and technology. In quantum dynamics, even a small number of periodically-driven spins leads to complicated dynamics. Hence, it is of interest to understand what constraints such dynamics must satisfy. We derive a set of constraints for each number of cycles. For pure initial states, the observable being constrained is the recurrence probability. We use our constraints for detecting undesired coupling to unaccounted environments and drifts in the driving parameters. To illustrate the relevance of these results for modern quantum systems we demonstrate our findings experimentally on a trapped-ion quantum computer, and on various IBM quantum computers. Specifically, we provide two experimental examples where these constraints surpass fundamental bounds associated with known one-cycle constraints. This scheme can potentially be used to detect the effect of the environment in quantum circuits that cannot be classically simulated. Finally, we show that, in practice, testing an n -cycle constraint requires executing only $O(\sqrt{n})$ cycles, which makes the evaluation of constraints associated with hundreds of cycles realistic.

The dynamics of isolated quantum systems become too hard to simulate on a classical computer or solve analytically when more than a few dozen spins are involved. Yet, the unitary evolution that characterizes isolated quantum systems is not arbitrary. It conserves purity, the von Neumann entropy, and any other function that depends on the eigenvalues of the density matrix. However, these conserved quantities are impractical since state tomography or other non-scalable techniques are typically needed to evaluate them. Here we study isolated quantum systems under periodic driving for two reasons. First, to gain a fundamental understanding of how the unitarity of isolated quantum systems restricts the evolution of observables, and second, to show the relevance of these restrictions to noise detection in state-of-the-art quantum computers. We start from the question: is the evolution of observables in a periodically-driven system more restricted compared to non-periodic driving? While it seems intuitively true, to the best of our knowledge no such constraints have been shown. We derive such constraints and show that these inequalities are more restrictive than other known bounds, which do not exploit periodicity. In Sec. 1 we introduce and derive the periodicity inequalities, and in section 2 we experimentally demonstrate their added value by exploring pure and mixed-state scenarios that are challenging for existing bounds as described below.

Constraints on observables that are valid for arbitrary driving have been derived within the frameworks of stochastic and quantum thermodynamics. These constraints include, the second law in quantum microscopic setups fluctuation theorems [1, 2, 3], thermodynamic uncertainty relation [4, 5, 6, 7], passivity based constraints [8, 9, 10], and more. We do not include constraints that involve non-observable, information-like, quantities as in resource theory and other frameworks [10, 11]. As it turns out, thermodynamic constraints lose their predictive power in the zero-temperature limit [12, 13, 14]. In appendix I, we show this explicitly for the second law and the Jarzynski fluctuation theorem. However, in quantum computers and simulators the input state is

Raam Uzdin: tanmoy.pandit@huji.ac.il, raam@mail.huji.ac.il

typically pure, which makes many thermodynamic-based constraints unsuitable for evolution-noise detection. Another challenge for thermodynamic-like constraints involves coherence in the energy basis. Fluctuation theorems, for example, are based on the two-point measurement scheme. The first measurement is carried on the initial state, which leads to wavefunction collapse. Crucially this measurement changes the evolution from a unitary evolution to a mixture of unitaries.

We show the added value of our inequalities by: i) demonstrating that the periodicity bounds can detect violation of periodicity even if the system is isolated; ii) showing that the periodicity constraints remains useful for detecting unaccounted coupling to an environment, in the zero-temperature limit; iii) breaking a recently derived bound on the maximal temperature of detectable environments.

Preliminaries: A Simple Inequality For Unitary Evolution

Let ρ_f be the density matrix that is obtained from ρ_0 by unitary transformation. Due to the non-negativity of the L2 norm it holds that,

$$\text{tr}[(\rho_0 - \rho_f)^2] \geq 0,$$

Next, we expand this expression and use the cyclic property of the trace to obtain the following form

$$\text{tr}[\rho_0^2] + \text{tr}[\rho_f^2] - 2\text{tr}[\rho_0\rho_f] \geq 0, \quad (1)$$

Since the evolution $\rho_0 \rightarrow \rho_f$ is unitary, the purity is conserved, $\text{tr}[\rho_0^2] = \text{tr}[\rho_f^2]$, and we obtain

$$\text{tr}[\rho_0(\rho_0 - \rho_f)] \geq 0. \quad (2)$$

Next, we use the fact that for unitary evolution purity conservation can be generalized to any trace value $\text{tr}[(\rho_0 - aI)^2] = \text{tr}[(\rho_f - aI)^2]$ where I is the identity operator and a is any real number. The proof follows trivially by expanding the parentheses. Thus, if r_0 is some Hermitian operator (potentially traceless) and evolves unitarily to r_f , i.e. $r_f = Ur_0U^\dagger$ where U is a unitary matrix, then by repeating the steps that lead to (2) together with $\text{tr}[r_0^2] = \text{tr}[r_f^2]$ we obtain

$$\text{tr}[r_0(r_0 - r_f)] \geq 0. \quad (3)$$

1 Periodicity inequalities

1.1 The two-cycle inequality

Next, we consider a periodically-driven system, i.e. the density matrix after each cycle satisfies

$$\rho_{k+1} = U\rho_kU^\dagger, \quad (4)$$

where U is a unitary evolution operator. The fact that U does not depend on k reflects the assumption of periodic driving. From linearity, it follows that the object

$$r_0 = \sum_{j=0}^N \alpha_j \rho_j, \quad (5)$$

where $\alpha_j \in \mathbb{R}$ and ρ_j is the density matrix after j cycles, also satisfies $r_{k+1} = Ur_kU^\dagger$. In the following, we use the term ‘stencil’ for r . According to (3) it holds that

$$\text{tr}[r_0(r_0 - r_M)] \geq 0, \quad (6)$$

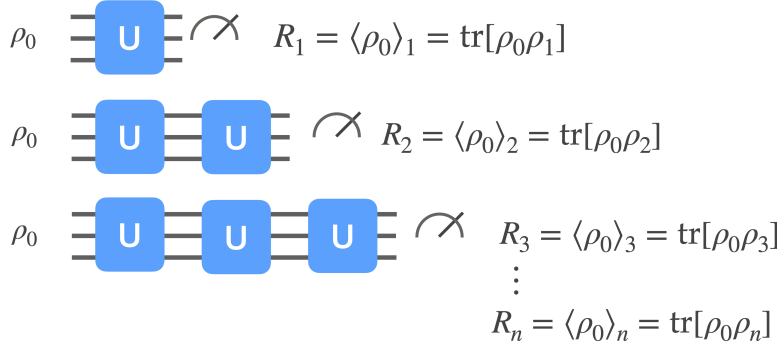


Figure 1: Illustration of the protocol for obtaining the k cycle recurrence probability R_k which appears in the periodicity inequalities [eqn. (11)-(13) etc.]. The recurrence probability R_k expresses to what extent the system has returned to its initial state after k cycles. The different R_k are statistically independent, and the measurement of R_k do not affect $R_{j>k}$ since they are evaluated in different experiments. Hence, despite the quantum evolution and the multiple measurements in this protocol, there is no wavefunction “collapse” that modifies the evolution.

where $r_M = U^M r_0 U^{\dagger M}$. Consider the simple case where $r_0 = \rho_1 - \rho_0$, and $r_M = r_1 = \rho_2 - \rho_1$, the inequality (6) leads to

$$\begin{aligned}
 0 &\leq \text{tr}[(\rho_1 - \rho_0)(-\rho_0 + 2\rho_1 - \rho_2)] \\
 &= \text{tr}[\rho_0^2] + 2\text{tr}[\rho_1^2] - 3\text{tr}[\rho_0\rho_1] \\
 &\quad - \text{tr}[\rho_1\rho_2] + \text{tr}[\rho_0\rho_2].
 \end{aligned} \tag{7}$$

$R_k = \text{tr}[\rho_0\rho_k]$ is the key quantity in our work and we shall refer to it as the *recurrence probability*. For a pure state, ρ_0 is the projector on to the initial state, $\rho_0 = |\phi_0\rangle\langle\phi_0|$. Therefore, $\text{tr}[\rho_0\rho_k]$ is the probability to measure the system in the initial state $|\phi_0\rangle$ after k cycles. R_k is an inner product, and can therefore be thought of as the amount of overlap with the initial state even for mixed ρ_0 . That is, R_k still expresses to what extent the density matrix returns to its initial value after k cycles.

Using purity conservation in unitary evolution, $\text{tr}[\rho_0^2] = \text{tr}[\rho_1^2]$, it holds that

$$3R_0 - 3R_1 - \text{tr}[\rho_1\rho_2] + R_2 \geq 0. \tag{8}$$

However, $-\text{tr}[\rho_1\rho_2]$ is presently in an inconvenient form as both ρ_1 and ρ_2 are unknown. To overcome this we use the fact that the driving is periodic,

$$\begin{aligned}
 \text{tr}[\rho_j\rho_{j+k}] &= \text{tr}[\rho_j U^j \rho_k U^{\dagger j}] \\
 &= \text{tr}[U^{\dagger j} \rho_j U^j \rho_k] \\
 &= \text{tr}[\rho_0\rho_k] = R_k.
 \end{aligned} \tag{9}$$

Applying eq. (9) in eq. (8) we get

$$R_2 - 4R_1 + 3R_0 \geq 0, \tag{10}$$

which is the simplest inequality in our approach since it contains only two cycles, or three time points including the initial state. Periodicity was assumed for the driving and the density matrix does not evolve periodically in the general case. Note that the coefficients in (10) sum up to zero. When the evolution is the identity operator, so that $R_k = 1$, this property leads to a saturation of the inequality 10 of the form $0 \geq 0$.

Operationally, the inequality in (10) is evaluated as illustrated in Fig. 1. The R_0 measurement can be skipped if the state preparation and measurement errors (SPAM) are negligible. After the initial state is evolved for one cycle, R_1 is measured. Next, in a third set of measurements, R_2 is measured, and so on.

Note that the one-cycle inequality $R_0 \geq R_1$ becomes trivial for pure states since $R_0 = 1$ and $1 \geq R_1$ always holds as the recurrence probability cannot exceed one. In contrast, (10) provides a non-trivial prediction for pure ρ_0 , which is a typical starting point for quantum devices. In Appendix II, we further discuss the two-cycle inequality and its added value for mixed states.

1.2 A recipe for constructing multi-cycle inequalities

The following recipe can be used to obtain more general periodicity bounds:

- Choose a stencil of the form $r_0 = \sum_{j=0}^N \alpha_j \rho_j$ (α_i are real numbers).
- Choose M to set the shift value in $r_M = U^M r_0$.
- Expand the parenthesis in $\text{tr}[r_0(r_0 - r_M)] \geq 0$.
- Replace $\text{tr}[\rho_m \rho_{m+k}] \rightarrow R_k = \text{tr}[\rho_0 \rho_k]$.

The last stage includes the $m = 0$ case: $\text{tr}[\rho_k^2] \rightarrow R_0 = \text{tr}[\rho_0^2]$. The number of cycles is determined by largest index of R_k that appears in r_M . Thus the number of cycles in the resulting inequality is $n = N + M$.

1.3 The discrete derivative inequalities S_n

The two-cycle inequality (10) was obtained by using the stencil $r_0 = \rho_1 - \rho_0$ which has the form of a first-order discrete time derivative. Next, we exploit higher-order discrete derivative to generate additional stencils. We denote by $r_0^{(n)}$ the shifted discrete derivative $r_0^{(1)} = \rho_1 - \rho_0, r_0^{(2)} = \rho_2 - 2\rho_1 + \rho_0, \dots$. The second derivative $r_0^{(2)}$ is centered at $k = 1$, The third derivative is centered at $k = 2$ and so on. This shift ensures that the derivative does not include negative indices. For r_M we choose r_1 . Applying the recipe in Sec. (1.2) to the stencils $r_0 = (\frac{1}{2})^n r_0^{(n-1)}$, and denoting the resulting inequalities by S_n where n is the number of cycles, the first few inequalities are

$$S_2 = \frac{1}{8}(R_2 - 4R_1 + 3R_0) \geq 0, \quad (11)$$

$$S_3 = \frac{1}{32}(-R_3 + 6R_2 - 15R_1 + 10R_0) \geq 0, \quad (12)$$

$$S_4 = \frac{1}{128}(R_4 - 8R_3 + 28R_2 - 56R_1 + 35R_0) \geq 0. \quad (13)$$

The S_n inequalities can be written as $S_n = \sum_{k=0}^n w_k^{(n)} R_k \geq 0$ where the coefficients $w_k^{(n)}$ alternate sign as a function of k and satisfy $\sum_{k=0}^n w_k^{(n)} = 0$ and $\sum_{k=0}^n |w_k^{(n)}| = 1$. As shown later, when n is sufficiently large the coefficients take the form: $w_k^{(n)} \rightarrow \frac{(-1)^k}{\sqrt{\pi n}} e^{-\frac{k^2}{n}}$.

1.4 Low-cost evaluation of the S_n periodicity inequalities

We introduce the notation $A_{\pm} \rho_n = \rho_{n \pm 1}$, and show in Appendix III that the S_n inequalities can be written as

$$S_n = \text{tr}[\rho_0 (\frac{1}{2} - \frac{1}{4}A_- - \frac{1}{4}A_+)^n \rho_0]. \quad (14)$$

The expression $(\frac{1}{2} - \frac{1}{4}A_- - \frac{1}{4}A_+)^n$ describes a classical n -step random walk with probability 1/4 to move one step forward, 1/4 to move one step backward, and 1/2 to stay in place. For large n , the probability distribution for moving moving k steps forward is given by the normal distribution with single-step variance σ_0^2 :

$$\frac{1}{\sqrt{2\pi\sigma_0^2 n}} e^{-\frac{k^2}{2\sigma_0^2 n}} = \frac{1}{\sqrt{\pi n}} e^{-\frac{k^2}{n}}, \quad (15)$$

where we have used: $\sigma_0^2 = \frac{1}{2} \cdot 0 + 2 \cdot \frac{1}{4} \cdot 1 = \frac{1}{2}$. Applying this result to eq. (14) we find

$$\begin{aligned} S_n &= \sum_{k=-n}^n \frac{(-1)^k}{\sqrt{\pi n}} e^{-\frac{k^2}{n}} R_{|k|} \\ &= \frac{1}{\sqrt{\pi n}} R_0 + 2 \sum_{k=1}^n \frac{(-1)^k}{\sqrt{\pi n}} e^{-\frac{k^2}{n}} R_k. \end{aligned} \quad (16)$$

Expression (16) suggests that the coefficients $w_k^{(n)}$ decay very fast as a function of k and therefore the series S_n can potentially be truncated at some value L without significantly changing the value of S_n . Operationally, it means that fewer than n cycles are needed for evaluating S_n . This is a useful feature for detecting small evolution noise, that may require evaluating S_n with large n .

Next, we set a bound on the error incurred by truncating the sum at $L < n$.

$$\begin{aligned} \sum_{k=L}^n \frac{(-1)^k}{\sqrt{\pi n}} e^{-\frac{k^2}{n}} R_k &\leq \sum_{k=L}^n \frac{1}{\sqrt{\pi n}} e^{-\frac{k^2}{n}} \\ &\leq \sum_{k=L}^{\infty} \frac{1}{\sqrt{\pi n}} e^{-\frac{k^2}{n}} \\ &\simeq \frac{1}{2} \operatorname{erfc}\left(\frac{L}{\sqrt{n}}\right) \frac{1}{2\sqrt{\pi n}} e^{-\frac{L^2}{n}}. \end{aligned} \quad (17)$$

For convenience we set $L = \xi\sqrt{n}$ and get

$$2 \sum_{k=L}^n \frac{1}{\sqrt{\pi n}} e^{-\frac{k^2}{n}} \simeq \operatorname{erfc}(\xi) + \frac{1}{\sqrt{\pi n}} e^{-\xi^2}. \quad (18)$$

From (16) and (18) we finally obtain that $S_n^{(L)}$ the L -cycle truncated version of the S_n satisfies

$$\begin{aligned} S_n^{(L=\xi\sqrt{n})} &= S_n - \sum_{k=L}^n w_k R_k \\ &\geq -2 \sum_{k=L}^n \frac{1}{\sqrt{\pi n}} e^{-\frac{k^2}{n}} R_k \\ &\geq -\operatorname{erfc}(\xi) - \frac{1}{\sqrt{\pi n}} e^{-\xi^2}. \end{aligned} \quad (19)$$

This inequality should be used as follows: n is fixed by the S_n that needs to be evaluated, the required accuracy ϵ is used to determine ξ via $\epsilon = \operatorname{erfc}(\xi) + \frac{1}{\sqrt{\pi n}} e^{-\xi^2}$ and finally, the truncation value is $L = \xi\sqrt{n}$. For example, to get an error of 5×10^{-3} in the calculation of S_{1000} (1000 cycles), only $L = 64$ cycles need to be measured ($\xi = 2$). For an accuracy of 10^{-5} , 99 cycles are needed ($\xi = \pi$), and 126 measured cycles already yield an accuracy of 2×10^{-8} . We emphasize that in practice the accuracy is limited by statistical noise. For example in the experiment in section 2.3 the truncation error is 1/65 of the 3σ -width when taking 24 points ($\xi = 2.1$). For 30 points ($\xi = 2.63$), the truncation error is already 1/1000 of the 3σ width.

1.5 Optimized three-cycle inequality

In the following, we explore the continuum of three-cycle inequalities, i.e. we are not using the discrete derivative stencil as in the previous sections. The goal is produce bounds that can perform better at detecting evolution noise. Consider the general three-cycle stencil,

$$r_0 = \rho_0 + x\rho_1 + y\rho_2, \quad (20)$$

where x and y can take any real value. Using the recipe in Sec. 1.2 we get the following inequality:

$$\begin{aligned} L(x, y) &= -yR_3 + (-x + 2y - xy)R_2 \\ &+ (-1 + 2x - y - (x - y)^2)R_1 \\ &+ (1 - x + x^2 + y^2 - xy)R_0 \geq 0. \end{aligned} \quad (21)$$

We notice that the left hand side, which we denote by $L(x, y)$, is a second-order polynomial in x and y , where the coefficients of $x, y, xy, x^2, y^2, 1$ depend on $\{R_n\}_{n=0}^3$.

If the evolution is unitary and periodic, $L(x, y) \geq 0$ for any value of x and y . Yet, in the presence of evolution noise, $L(x, y)$ might be positive for some choices of x and y and negative for other choices. It is also possible that $L(x, y)$ is not negative for any choice of x and y . In that case, the evolution noise is not detectable with four-point periodicity inequalities. To test if the noise is detectable we check if $\min_{x,y}[L(x, y)] < 0$ by finding the optimal x and y that minimize L .

In a given physical scenario that consists of an initial condition and a driving protocol, $\{R_n\}_{n=0}^3$ are just constant positive numbers and $L(x, y)$ is a second-order polynomial with known and fixed coefficients. Next we check which type of paraboloid $L(x, y)$ is. Evaluating the second-derivative test for a paraboloid $\partial_x^2 L \partial_y^2 L - (\partial_x \partial_y L)^2 \geq 0$, we find $\partial_x^2 L \partial_y^2 L - (\partial_x \partial_y L)^2 = (R_0 - R_1)(3R_0 - 4R_1 + R_2) = 8(R_0 - R_1)S_2$. If $S_2 < 0$ it means that $L(x, y)$ is hyperbolic paraboloid and for some value of x, y it must be negative. $L(x, y) < 0$ implies detection, but this is not surprising since the noise is already detectable with two cycles since $S_2 < 0$. S_2 corresponds to $x = -1, y = 0$. The more interesting case is $S_2 > 0$ where $L(x, y)$ is a paraboloid. Now detection $L(x, y) < 0$ is not guaranteed. Furthermore, the motivation for using an optimized bound for evolution noise detection is that S_2 and S_3 , which use $\{R_n\}_{n=0}^3$, failed to detect it. To determine if $L(x, y)$ is a convex or concave paraboloid we check the limit $x \rightarrow \infty, y = 0$. Since $L(x, y)$ is positive in this limit we conclude $L(x, y)$ is convex. Consequently, the most negative value of $L(x, y)$ occurs when $\partial_x L(x, y) = 0$ and $\partial_y L(x, y) = 0$, we denote the solution to these two equations by x_{min} and y_{min} . Finding x_{min}, y_{min} we get that $L(x_{min}, y_{min}) \geq 0$ is equal to

$$\frac{(2R_0 - R_1 - 2R_2 + R_3)}{(R_0 - R_2)(3R_0 - 4R_1 + R_2)} (R_0^2 - R_0(R_1 + R_3) - (R_1 - R_2)^2 + R_1 R_3) \geq 0. \quad (22)$$

This bound is non-linear in the expectation values R_k since these expectation values are being used to choose the optimal x and y for detection. If the inequalities that involve R_0, R_1 and R_2 hold, i.e. $R_0 - R_2 \geq 0$ and $3R_0 - 4R_1 + R_2 \geq 0$, then the non-linear bound (22) simplifies to

$$R_0^2 - R_0(R_1 + R_3) - (R_1 - R_2)^2 + R_1 R_3 \geq 0. \quad (23)$$

The non-linearity in this inequality is different from the density matrix non-linearity that is usually considered in quantum information and quantum thermodynamics (e.g. purity, von Neumann entropy $S_{vn} = -tr[\rho \ln \rho]$, etc.) as here it appears outside the trace. An experimental measurement of this inequality is given in Sec. 2.4.

While optimized bounds become more burdensome to derive as the number of cycles increases, the existence of these bounds can enable the detection of violations with a relatively small number of measurements.

2 Numerical and Experimental demonstrations

We present numerical simulations and experimental results from IBM superconducting quantum processors and a trapped ion quantum computer (TIQC). Each example illustrates a different feature of the new bounds.

2.1 Detecting parameter drift during the evolution

There are only two assumptions made in deriving the periodicity inequalities, unitarity and periodic driving. A violation of the periodicity inequalities can arise from breaking either one or both of these assumptions. In this section we confirm that a non-periodic shift in the control parameters would manifest as a violation of these bounds by numerically investigating such a possibility.

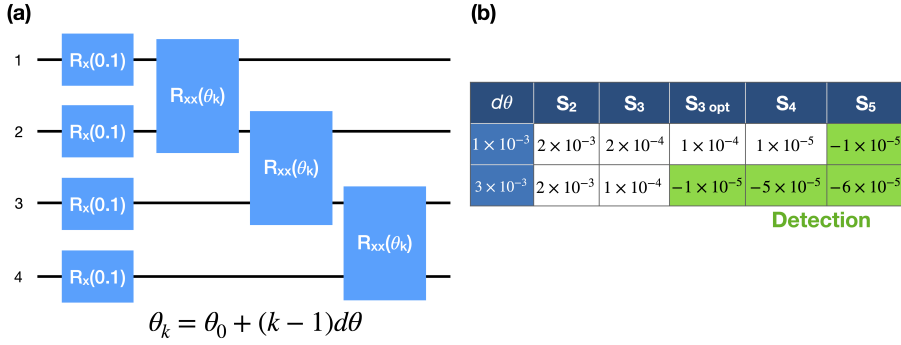


Figure 2: (a) In this circuit the $\sigma_x \sigma_x$ interaction (R_{xx}) changes from one cycle to the next (k dependence). (b) For a small drift of $d\theta = 10^{-3}$ the non periodicity is detectable after five cycles, i.e. $S_5 < 0$. When $d\theta = 3 \times 10^{-3}$, four cycles are enough for detecting the non-periodicity. Interestingly, it is possible to detect the non-periodicity by running only three cycles by applying the optimized 3-cycle periodicity inequality (23). To the best of our knowledge, the periodicity inequalities are the first constraints on unitary dynamics that are customized for periodic driving and as such the detection of non-periodicity is presently unique to these inequalities.

In Fig. 2a we numerically study a four-qubit system where the driving cycle is composed of four single-qubit rotations around the x-axis by angle of 0.1rad $R_x(0.1)$ where $R_x(\theta) = e^{-i\frac{1}{2}\theta\sigma}$ is a single qubit rotation around the x-axis of the Bloch sphere. These rotations are followed by nearest neighbor xx interactions between qubit j and qubit $j + 1$ that leads to the following evolution: $U_k^{[j,j+1]} = \exp[i\frac{\theta_k}{2}(\sigma_x^{(j)}\sigma_x^{(j+1)})]$. In order to simulate a drift of the control parameters, we chose $\theta_k = \theta_0 + (k - 1)d\theta$. $d\theta$ represents the drift of the parameter θ from one cycle to the next. The circuit is repeated for up to five cycles. Choosing $\theta_0 = 0.3$ rad and $d\theta = 10^{-3}$ rad, the first violation is observed after five cycles where $S_5 = -1.56 \times 10^{-5}$. If the drift is stronger, for example such that $d\theta = 3 \times 10^{-3}$ rad, the first violation is observed after three cycles when employing the three-cycle optimized inequality (23), which yields the value $S_{3 \text{ opt}} = -1.5 \times 10^{-5}$. The unoptimized three cycle bound yields $S_3 = +1.4 \times 10^{-4}$. Alternatively, an additional cycle can be used to detect the drift without resorting to an optimized bound $S_4 = -5.1 \times 10^{-5}$. Other values appear in Fig. 2b.

The violation of the periodicity inequality shown in this example highlights the power of these inequalities over thermodynamic bounds, which could only detect errors arising from non-unitarity. In this case, we detect the drift error in the device by exploiting tighter bounds arising from the periodicity of the intended evolution.

2.2 Evolution noise detection with a pure initial state

In some setups, such as digital quantum computers, pure-state initial conditions are more natural to use compared to mixed states, which require some dedicated preparation protocol (e.g. see [15] and [16]). It is natural, then, to ask if pure states can be used to detect evolution noise. Presently, constraints on observables in unitary dynamics are derived within the frameworks of stochastic and quantum thermodynamics. Thus, they are the relevant reference for the periodicity inequalities we present. Unfortunately, thermodynamic constraints become impractical to use when the initial state is sufficiently pure. As discussed in Appendix I, some thermodynamic inequalities become so loose that no evolution noise can violate them. In other thermodynamic constraints, the resources needed for evaluating and measuring them diverge as the initial state becomes pure. Hence, thermodynamic constraints are presently not suitable for detecting evolution noise in quantum computers and simulators. The periodicity inequalities studied here are free from this limitation. We present a proof-of-principle experiment for evolution noise detection using pure states. Our setup, shown in Figure 3(a), is composed of a two-qubit system coupled to a one-qubit environment ('e'). The initial state is created by single-qubit gates, which are not shown in the figure. The single cnot gate between the upper two qubits constitutes the periodic unitary driving. While this environment is artificial, it has the advantage that we can easily decouple it from the system and verify that there is no noise detection in this case.

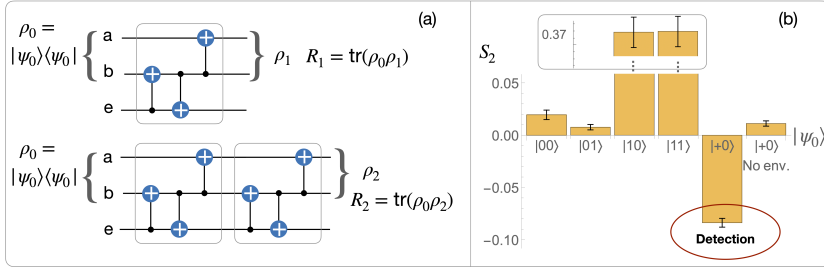


Figure 3: (a) a circuit for demonstrating heat leak detection with a pure initial state. The initial condition is $|\psi_0\rangle\langle\psi_0|$ in the upper two qubits which constitute the system and the bottom environment qubit is initially in $|0\rangle\langle 0|$. The recurrence probability of the two upper spins is measured after one cycle in one experiment, and after two cycles in a different experiment. (b) The experimental values of S_2 for various input states carried out on the IBM Bogota processor. The negative value for $|\psi_0\rangle = |+_a 0_b\rangle$ indicates the detection of the environment. When the environment is decoupled for the same input state (“No env.” in the figure) S_2 yields a positive value as expected. This experiment illustrates detection of evolution noise using pure state which is impossible in thermodynamically-inspired frameworks.

The experiment is composed of three sub-experiments for measuring R_0, R_1 and R_2 . We test several different input states: $|00\rangle, |01\rangle, |10\rangle, |11\rangle$, and $|1+\rangle$. Our goal is to observe a violation of S_2 when the environment is connected, and no violation when it is not. Figure 3(b) shows that states in the computational basis cannot detect the evolution noise but the superposition state in the computation basis $|1+\rangle$ can. The error bars correspond to $\pm 3\sigma$ statistical uncertainty. The last bar in Figure 3(b) shows that, as expected, when the environment qubit is decoupled S_2 is positive and there is no detection. That is, we confirm that our inequality does not always yield negative values regardless of the coupling to the environment qubit.

Interestingly, the circuit is completely classical for binary input, i.e. diagonal states in the computational basis. In this case, it acts as a simple permutation in the computation basis $0_a 1_b \leftrightarrow 1_a 1_b$. The positive values for all four elements of the computation basis [Fig. 3(b)] imply that no classical binary input (including stochastic inputs with classical correlations) can be used to detect the noise induced by the environment qubit ‘e’, in this circuit. Yet, a quantum superposition of two classical binary states can detect the coupling to the environment. While this example does not involve a strong quantum feature, such as entanglement, it naturally raises the question if entangled states can lead to detection of noise that cannot be detected using classically-correlated states. The key point of this experiment is the demonstration of noise detection using a unitary constraint when starting in a pure state. A task that, to the best of our knowledge, is not possible using the known thermodynamic constraints.

To conclude this section we point out that while a violation indicates a deviation from a perfect periodic unitary driving, isolating the cause such as parameter drift, decoherence, spontaneous emission, or other evolution noise mechanisms, requires further tests.

2.3 Detection of realistic noise

Following the controlled artificial environment demonstration above, it is interesting to check whether this method can detect the real physical environment of quantum processors. The following experiment shows that the real environment is indeed detectable when exploring larger numbers of cycles. The one-cycle circuit we use is shown in the inset of Fig. 4 where $\theta = 1$. The value of θ was chosen arbitrarily and it is not optimal. Other values might detect weaker evolution noise or to observe a violation with fewer cycles. Qubits 1 and 2 of the IBM Santiago processor are initialized in the state $|00\rangle$. Figure 4(a) shows the values of S_n as a function of the number of cycles. The width of the line corresponds $\pm 3\sigma$ uncertainty. Hence, starting from 17 cycles, one can see a violation beyond the 3σ uncertainty. This result shows that these inequalities can detect the intrinsic processor noise when using a pure state as the input state.

Figure 4b shows the results of a similar experiment carried out on the IBM Casablanca processor, for 65 cycles and $\theta = 0.1$. The value of θ was modified from the previous experiment as we now wish to demonstrate the utility of the scaling feature presented in Sec. 1.4. In this

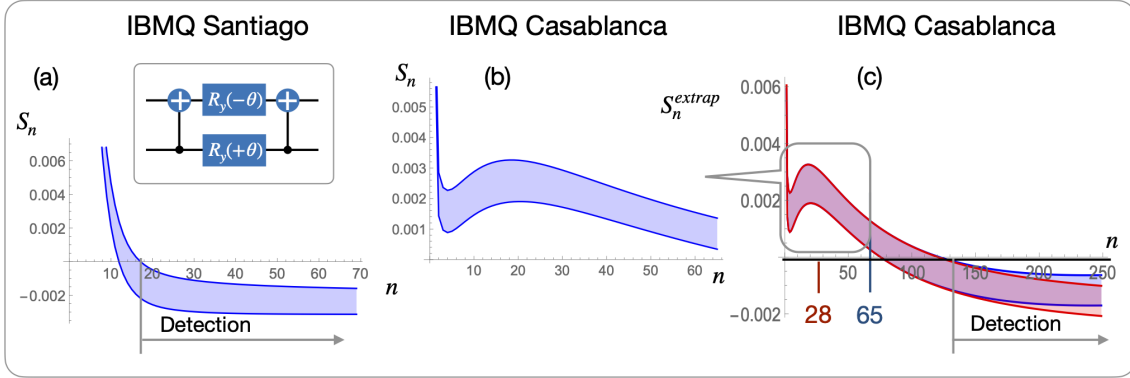


Figure 4: Inset: the circuit used for evaluating the S_n inequalities under the intrinsic noise of the IBM processors. The initial condition is the ground state. R_y is a single qubit rotation around the y axis. (a) For qubits 2 & 3 of the Santiago processor and $\theta = 1.0$, the environment leads to a violation after 17 cycles, i.e. $S_{17} < 0$. (b) Running the same experiment on qubits 5 & 6 of the Casablanca processor and $\theta = 0.1$, no violation is observed for the 65 cycles we were able to run in this experiment. (c) Using the extrapolation described in Sec. 1.4 based on the favorable \sqrt{n} scaling, a violation is observed after 130 cycles. The extrapolation can be used to detect a heat leak using the first 65 cycles (blue) or even just the first 28 cycles (red).

case, there is no violation within the number of cycles measured, but it seems that if more cycles were measured a violation could have been observed. Fortunately, from the analysis in Sec. 1.4 we know that for large enough n the contribution of the last cycles decays like a gaussian in the number of cycles $w_k^{(n)} \propto e^{-k^2/n}$. Consequently, only the first $\xi\sqrt{n}$ terms contribute to the value of S_n . ξ is roughly 3 but its exact value depends on the required accuracy of the clipped sum with respect to the full sum. This suggests the 65 cycles we have measured can be used to evaluate S_n with $n > 65$. Setting $\xi = \pi$ and $M = 65$, we can extrapolate up to $\lfloor (65/\pi)^2 \rfloor = 428$ with an error of 10^{-5} , which is not observable on the scale of Fig 4c. The blue curve, which overlaps with the red curve until $n \sim 140$, is generated by taking the measured $\{R_k\}_{k=0}^{65}$ and setting $R_k = 0$ for $k \geq 66$ in the expression for S_n . We find negative values that indicate the presence of evolution noise starting from $n = 130$. We conclude that the noise is detectable with only 65 cycles. This illustrates the efficiency of the S_n inequalities.

It seems that perhaps even 65 samples are more than enough for observing the violation. The red curve is S_n with R_k data from only 28 cycles. The red band shows extrapolation based on only 28 points. According to eq. (18) at 140 cycles, for example, the error should be smaller than 1×10^{-3} , which is too big to confirm a violation. Yet, in practice, at $n = 140$ the extrapolation based on 28 points is almost indistinguishable from the one exploiting 65 points. The bound given in eq. (18) on the truncation error of S_n is rather loose since it assumes that the signs of the coefficients $w_k^{(n)}$ do not alternate as a function of k , and that all recurrence probabilities are one. Thus, in practice, the contribution of the terms with high cycle number to the sum can be much smaller. In general, it is possible to start with a small number of cycles, and then add more cycles until convergence is achieved at the extrapolated point. Potentially, other initial states can lead to earlier detection of evolution noise, but the goal of this example is to illustrate the advantage of the \sqrt{n} scaling and not to find the optimal detection scheme.

2.4 Noise Detection Beyond the Hot-Environment Limit

Evolution noise created by hot environments deserves special attention. In the extreme case where the environment is fully mixed, i.e. infinite temperature, the observed system experiences unital dynamics. Unital maps are characterized by the fact that the fully-mixed state is a fixed point of these maps [17, 18]. Decoherence processes are another example of unital map. For practical purposes, it is enough that the temperature is significantly larger than the energies of the system. Although not unitary, unital dynamics are consistent with second-law-like inequalities [19, 20, 14] and passivity-based inequalities [21, 8, 9]. Thus, unital dynamics cannot violate these inequalities, and therefore these inequalities cannot be used to detect unital noise. One can expect that if the

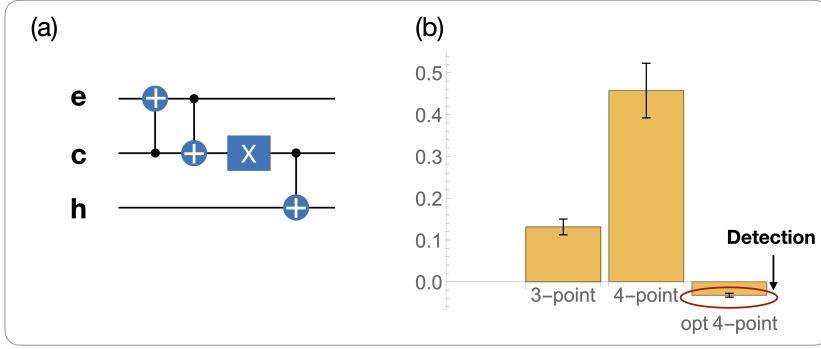


Figure 5: An experiment that confirms the capability of the periodicity inequalities to detect hot environments which cannot be detected using two-point passivity-based bounds [see eq. (25)]. Running the circuit (a) for two and three cycles, we observe in (b) that the S_2 and S_3 inequalities are not violated, but the optimized three-cycle inequality is violated and therefore confirms the coupling to the hot qubit 'e'. The experiment was done on the Ourense IBM processor. See main text for details.

environment is slightly less hot so that the system thermalizes to a state, which slightly deviates from a fully mixed state, it will still be hard to detect the noise this environment induces on the system. In Ref. [9] a theorem was derived on the environment temperature T_{env} that can still be detected: there is no observable C in the Hilbert space of the system that satisfies

$$\langle C \rangle_{final} - \langle C \rangle_{inial} \geq 0, \quad (24)$$

for any unitary or unital transformation, that can yield $\langle C \rangle_{final} - \langle C \rangle_{inial} \leq 0$, i.e. be violated, when the system is coupled to temperature $T_{env} > T_{undetec}$ where

$$T_{undetec} = \frac{\max(E_{env}) - \min(E_{env})}{\min(\mathcal{B}_n^{vis} - \mathcal{B}_{n-1}^{vis})}, \quad (25)$$

$\{E_{env}\}$ are the energy levels of the environment, and \mathcal{B}_n^{vis} is the n -th eigenvalue of $-\ln \rho_{sys}^{initial}$ (sorted in an increasing order of their size). Hence, if the temperature of the environment exceeds T_{undet} , it is undetectable by inequalities of the form (24). However, this bound is based on the one-cycle scheme with just one final state, in contrast to the multi-cycle approach presented in this paper. Thus, the periodicity inequalities have the potential to detect this type of environment. In the following experiment, we use the circuits shown in Figure 5(a). To generate thermal qubits for the environment and the system, an ensemble of pure states is used (see [15]). The inverse temperatures $\beta_h = 0.6$, $\beta_c = 3.5$ and $\beta_e = 0.5$ are chosen so that the condition given in eq. (25) guarantees that the environment is too hot to be detected using one-cycle inequalities on observables. As indicated by the negative value of the 3rd bar in Figure 5(b), by evaluating the optimized three-cycle inequality (23) the heat leak becomes detectable.

In summary, this experiment illustrates another added value of the periodicity inequalities with respect to similar inequalities, and that the optimized 3-cycle bound can detect environments that the S_3 cannot detect, although both of them use the same experimental data.

2.5 A three-qubit gate in trapped ions and superconducting circuits

Next, we explore the results of S_n for some common gates with simple outputs and consider the regime in which these results would provide benefit as diagnostic. Consider a gate U such as cnot, Toffoli (ccnot), Fredkin (cswap), etc. that satisfies $U|\psi_A\rangle = |\psi_B\rangle, U|\psi_B\rangle = |\psi_A\rangle$ i.e. U is a two-state permutation so that U^2 is the identity operator. If the initial condition is $\rho_0 = |\psi_A\rangle\langle\psi_A|$ or $\rho_0 = |\psi_B\rangle\langle\psi_B|$, the ideal output is $R_n = \{1, 0, 1, 0, 1, \dots\}$. As a result $S_n = \sum_{k=0}^{\lfloor n/2 \rfloor} w_{2k} = 1/2$. When the predicted R_n is so simple, there are many ways to quantify the deviation of the device from its expected behavior. For example, one can use $|R_n^{exp} - R_n|$. However, this quantity is always positive and a large value of $|R_n^{exp} - R_n|$ can appear due to coherent error, e.g. miscalibrated gates

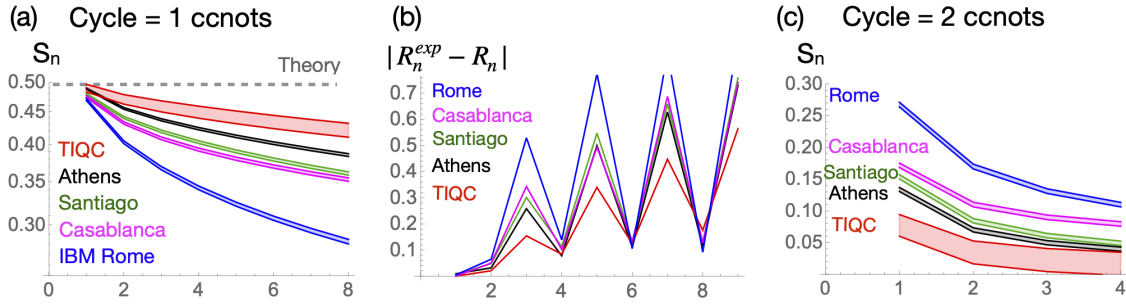


Figure 6: When a circuit changes the initial state to an orthogonal state, and in the next cycle returns to the initial state it holds that $S_n = 1/2$. (a) S_n values for various quantum processors where the circuit contains a single Toffoli gate. The plot shows that the TIQC exceeds the performance of various IBM processors which are further away from $1/2$. (b) The comparison of the theoretical and experimental values of the recurrence probabilities, $|R_n^{exp} - R_n|$, seems like a reasonable choice for comparing different processors. Yet, this quantity strongly fluctuates and in this case, no processor is consistently better at all time points. In contrast, the S_n shows a clear and consistent difference between the various processors. (c) Same as (a), but this time the cycle contains two consecutive Toffoli gates. In this case, the ideal evolution yields $S_n = 0$. Here as well, the TIQC performs better than the tested IBM superconducting quantum processors.

that change the intended unitary. Thus, $|R_n^{exp} - R_n|$ may not be associated with noise created by an environment. In contrast, negative values of S_n are a clear indication of evolution noise.

In our last experiment, we run sequentially the Toffoli gate with the initial state $|1_A 1_B 0_C\rangle$ where A and B are the controlling qubits. The experiment is carried out both on the IBMQ superconducting processors and on a TIQC. The TIQC results are obtained on the University of Maryland Trapped Ion (UMDTI) quantum computer, which is described in [22]. This experiment is performed using a linear chain of five $^{171}\text{Yb}^+$ ions in a room-temperature Paul trap under ultrahigh vacuum with the qubit encoded in two hyperfine ground states of Yb^+ . We re-analyze raw data from results reported in [23], where three of the five ions are treated as qubits while the others remain idle. For more information on the UMDTI hardware, see Appendix IV.

Figure 6(a) shows the S_n plots for various IBM processors and the UMDTI as a function of the number of cycles n . The $|R_n^{exp} - R_n|$ deviation with respect to the ideal output is depicted in Figure 6(b). While the $|R_n^{exp} - R_n|$ fluctuates, the S_n curves are monotonically decreasing. Using tools that are beyond the present paper one can prove that the S_n series must monotonically decrease if the evolution is unitary and periodic [24, 25]. On the other hand, the fluctuations of $|R_n^{exp} - R_n|$ and other measures, which are based on distance from the expected output, may be artificial. For example, if the noise is caused by spontaneous emission, the initial state is an excited state, and the ideal recurrence probabilities are $R_n = \{1, 0, 1, 0, \dots\}$, then for odd n values, the noise will decrease $|R_n^{exp} - R_n|$ as it will take the system closer to the ground state and reduce the overlap with the initial excited state. Note that the deviation from $1/2$ in Figure 6(b) can arise from a coherent error in the implementation. It appears that the TIQC data is the closest to the predicted $1/2$ value. Thus, an increase in the S_n plot is an indication for evolution noise, which is not observed here.

In our next test, we group pairs of Toffoli gates as a single cycle. The recurrence probability for this two-Toffoli cycle is $R'_n = R_{2n} = \{1, 1, 1, \dots\}$. Since $\sum_{k=0}^n w_k^{(n)} = 0$ it follows that for an ideal evolution $S'_n = \sum_{k=0}^n w_k^{(n)} R_{2k} = \sum_{k=0}^n w_k^{(n)} = 0$ for all n . Figure 6(c), shows the experimental values of S'_n for the various quantum processors. The same trends as in Figure 6a are observed. Note that in 6(b) Casablanca is more noisy for $n=3$ and $n=7$ but it is the other way around for $n=5$. We conjecture that the reason there are strong fluctuations in $|R_k^{exp} - R_k|$ and even lack of consistency regarding which processor is more noisy is related to coherent errors. These findings indicate that it is advantageous to check the performance of devices in terms of S_n when the ideal values of R_k are $1, 0, 1, 0, \dots$ or $1, 1, 1, 1, \dots$ compare to direct evaluation of the individual R_k values, i.e. $|R_k^{exp} - R_k|$.

Concluding remarks

We have presented a set of multi-cycle inequalities valid for periodically-driven quantum systems. Presently, we do not claim that these bounds will mature into a practical method for diagnosing evolution noise in quantum circuits, but our results present a clear case that this research direction warrants further investigation. The goal of this paper is to show that it is possible to formulate constraints that are customized to periodic driving and that they have an added value with respect to other known constraints. The periodicity inequalities have three appealing features. The first is the operational advantage: they use pure states and only the recurrence probability is measured. The second is that they treat the circuits as black boxes. The third is the \sqrt{n} scaling law, which states that only the first $\propto \sqrt{n}$ cycles contribute to the S_n inequality.

The construction of S_n has additional potential beyond the inequalities studied in this paper. For example, we have shown it is directly related to purity loss and therefore may have further application beyond detecting evolution noise, e.g. for devising a simple protocol for entanglement entropy measurement [24, 25].

Going beyond digital quantum circuits, our method could find applications in other scenarios with periodic driving, such as the simulation of Floquet many-body systems which have applications in the study of time crystals [26] and prethermalization [27]. Typical experimental sequences allow the calculation of bound violations based on existing data, e.g. in [28].

R.U. is grateful for support from Israel Science Foundation (Grant No. 2556/20). A.M.G. is supported by a JQI Postdoctoral Fellowship. N.M.L. acknowledges financial support from NSF grant no. PHY-1430094 to the PFC@JQI, and the Maryland-ARL Quantum Partnership, grant no. W911NF1920181.

Appendix I - The Zero Temperature Problem in Thermodynamic Constraints

There is a broad family of thermodynamic and thermodynamically-inspired constraints. Reviewing how exactly the zero temperature problem manifests in each one is beyond the scope of the present paper. In this appendix, we give as examples the Jarzynski fluctuation theorem, the second law in microscopic quantum systems, and passivity-based inequalities. The Jarzynski equality in systems whose Hamiltonian returns to its initial value reads

$$\langle\langle e^{-\beta W} \rangle\rangle = \sum p_i p_{i \rightarrow j} e^{-\beta(E_j - E_i)} = 1,$$

where $p_{i \rightarrow j}$ is the transition probability generated by the unitary driving, and W is the work invested in creating this transition. It is tempting to ignore all input states save the ground state, which is solely occupied in the $\beta \rightarrow \infty$ limit, however, the exponentially small probabilities are multiplied by an exponentially large factor (e.g. in the transition to the ground state from some other input state). Thus, all input states are important in the ultra-cold limit. This manifests in an exponentially diverging number of shots [13]

$$N = e^{\beta \langle W \rangle},$$

which makes this scheme impractical for pure-state initial conditions.

The second law in microscopic systems and passivity inequalities

For an isolated system that starts in thermal equilibrium the relevant statement of the second law is: energy cannot be extracted by applying a periodic force on the system. The translation to quantum systems is as follows: given a time independent system Hamiltonian H_s the initial density of the system is the Gibbs state

$$\rho_\beta = e^{-\beta H_s} / \text{tr}[e^{-\beta H_s}], \quad (26)$$

where β is the inverse temperature. A periodic driving force refers to a periodic driving Hamiltonian $V(t)$ that satisfies $V(t) = V(\tau) = 0$ where τ is the end of the process. The accumulated effect of

the time dependent Hamiltonian $H = H_s + V(t)$ can be described by a unitary evolution operator, such that the final density matrix is $\rho_0 = U\rho_\beta U^\dagger$. The second law in the case states that the final average energy of the bare Hamiltonian is equal to or larger than that of the initial state,

$$\langle H_s \rangle_f = \text{tr}[\rho_f H_s] \geq \text{tr}[\rho_\beta H_s] = \langle H_s \rangle_\beta. \quad (27)$$

This result can be derived in several ways. In particular, it is a special case of the Clausius-like inequalities for small quantum systems ([14] and references therein).

When β is finite this statement is not trivial because the excited states are populated according to (26). Thus, the system can reduce its energy by moving population to lower states. However, it turns out the unitary transformation (created by the periodic driving) cannot do that. Non-unitary dynamics, such as cooling can reduce the energy but this always involves heating up some other object. Thus, an experimental violation of (27) can be used to deduce that the system is not sufficiently isolated and interaction with an unaccounted environment takes place.

The key point in the context of this paper is that when $\beta \rightarrow \infty$, i.e. the ultra-cold limit, for all practical purposes only the ground state is initially populated. In this case, it does not matter if the dynamics are unitary or not, and if more objects are involved. The system is already in the minimum possible energy and therefore it can only increase. Since (27) cannot be violated in this case, it cannot be used to detect an environment.

A similar problem exists in passivity-based frameworks. In these framework the basic inequality stems from the passivity of the operator $B = F(\rho_0)$, where ρ_0 is the initial state and $F(x)$ is a monotonically-decreasing function in $x \in [0, 1]$. When $\beta \rightarrow \infty$, $\rho_0 \rightarrow |0\rangle\langle 0|$ and therefore the basic passivity inequality

$$\text{tr}[\rho_f B] - \text{tr}[\rho_0 B] \geq 0,$$

becomes trivially satisfied for pure states since $B = -|0\rangle\langle 0|$ (up to a multiplicative positive constant) for any F , and the passivity prediction is

$$\text{tr}[\rho_f |0\rangle\langle 0|] \leq 1,$$

which always holds even if the evolution is not unitary. Thus it cannot be used to detect non-unitary environments.

Appendix II - The Two-Cycle Inequality

As a basis for comparison, the usual one-cycle inequality, eq. (2), yields $R_0 \geq R_1$ and $R_0 \geq R_2$ which for pure states is trivial since $R_0 = 1$ and $R_0, R_1 \leq 1$. The inequality (10) can be assigned with different interpretations via different rearrangements:

$$R_2 \geq 4R_1 - 3R_0, \quad (28)$$

$$\frac{1}{4}(R_2 + 3R_0) \geq R_1, \quad (29)$$

$$(R_0 - R_1) \geq \frac{1}{4}(R_0 - R_2) \geq 0. \quad (30)$$

Inequality (28) provides a *lower* bound on R_2 (the two-point bound yields an upper bound $R_2 \leq R_0$), while (29) offers a refined upper bound on R_1 . Since $R_0 \geq \frac{1}{4}(R_2 + 3R_0)$ this bound is always tighter than the two-point bound $R_0 \geq R_1$. Interestingly this bound is using the information on R_2 , so the two endpoints are used for bounding the midpoint. Inequality (30) compares the change in the recurrence probability in the first half to the cumulative change $R_0 - R_2$. It suggests that the change cannot occur just in the second half of the evolution; at least a quarter must take place in the first half. Similarly one can write $3(R_0 - R_1) \geq R_1 - R_2$ and directly compare the two halves. Note however that in this form the right-hand side might become negative. Another added value of the form (30) is that it makes it easier to compare with the two-point inequalities $R_0 \geq R_1$ and $R_0 \geq R_2$. The inequality (30) shows that $R_0 - R_1$ is not just non-negative but also larger than another non-negative number, $\frac{1}{4}(R_0 - R_2)$. Thus, it is tighter than the two-point prediction $R_0 - R_1 \geq 0$.

Appendix III - Derivation of Equation (14)

The n -th discrete shifted derivative can be written $(1 - A_+)^n \rho_0$ where $A_+^n \rho_m = \rho_{m+n}$ and $A_-^n \rho_m = \rho_{m-n}$. Note, that A_+ and A_- commute. Using this notation S_n can be written as

$$S_n = \frac{1}{2^{2n}} \text{tr}[(1 - A_+)^{n-1} \rho_0 [(1 - A_+)^{n-1} - A_+ (1 - A_+)^{n-1} \rho_0]. \quad (31)$$

Next, we use the shift invariance property $\text{tr}[\rho_n \rho_m] = \text{tr}[\rho_0 \rho_{m-n}]$ to obtain

$$S_n = \frac{1}{2^{2n}} \text{tr}[\rho_0 (1 - A_-)^{n-1} [(1 - A_+)^{n-1} - A_+ (1 - A_+)^{n-1} \rho_0], \quad (32)$$

or

$$S_n = \frac{1}{2^{2n}} \text{tr}[\rho_0 (1 - A_-)^{n-1} (1 + A_-)^{n-1} (1 - A_+) \rho_0]. \quad (33)$$

Next, we apply the hermitian conjugate of the expression inside the trace. It still gives S_n since it is real but changes A_+ to A_- and vice versa and we get the alternative expression

$$S_n = \frac{1}{2^{2n}} \text{tr}[\rho_0 (1 - A_-)^{n-1} (1 + A_-)^{n-1} (1 - A_-) \rho_0]. \quad (34)$$

Combining Eq. (33) and Eq. (34) we get

$$S_n = \frac{1}{2^{2n}} \text{tr}[\rho_0 (1 - A_-)^{n-1} (1 + A_-)^{n-1} (2 - A_- - A_+) \rho_0]. \quad (35)$$

Finally, since $(1 - A_-)^n (1 - A_+)^n = (2 - A_- - A_+)^n$ we get eq. (14)

$$\begin{aligned} S_n &= \frac{1}{2^{2n}} \text{tr}[\rho_0 (2 - A_- - A_+)^n \rho_0] \\ &= \text{tr}[\rho_0 (\frac{1}{2} - \frac{1}{4} A_- - \frac{1}{4} A_+)^n \rho_0]. \end{aligned}$$

Appendix IV - The University of Maryland Trapped-Ion Quantum Computer

The UMDTI quantum computer is described in [22]. Briefly, two-photon Raman transitions are used to control the qubit state, encoded in two magnetic-field-insensitive hyperfine ground states of $^{171}\text{Yb}^+$ ions held in a linear chain in a Paul trap. Individual manipulation of each qubit is performed by splitting one of the Raman laser beams into several beams, each controlled by an independent acousto-optic modulator channel and focused onto a single ion in the chain. Single-qubit gate operations are executed by creating laser pulses of controlled phase and duration while two-qubit gates are compiled from single-qubit gates and a laser-driven entangling Ising gate (XX or $e^{i\lambda\sigma_x\sigma_x}$) following the Mølmer-Sørensen gate scheme [29, 30, 31], which creates entanglement between pairs of qubits via the shared harmonic oscillator modes of the ion chain in the trap. These modes act as an information bus with which the qubits are temporarily entangled. Modulation of the Raman beam amplitude is used to leave the qubits disentangled from these motional degrees of freedom at the end of the gate operation [32, 33].

References

- [1] Rosemary J Harris and Gunther M Schütz. Fluctuation theorems for stochastic dynamics. *Journal of Statistical Mechanics: Theory and Experiment*, 2007(07):P07020, 2007. DOI: [10.1088/1742-5468/2007/07/P07020](https://doi.org/10.1088/1742-5468/2007/07/P07020). URL <https://doi.org/10.1088/1742-5468/2007/07/P07020>.
- [2] Udo Seifert. Stochastic thermodynamics, fluctuation theorems and molecular machines. *Reports on progress in physics*, 75(12):126001, 2012.
- [3] Christopher Jarzynski. Equalities and inequalities: Irreversibility and the second law of thermodynamics at the nanoscale. *Annu. Rev. Condens. Matter Phys.*, 2(1):329–351, 2011. DOI: [10.1146/annurev-conmatphys-062910-140506](https://doi.org/10.1146/annurev-conmatphys-062910-140506). URL <https://doi.org/10.1146/annurev-conmatphys-062910-140506>.

- [4] Matteo Polettini, Alexandre Lazarescu, and Massimiliano Esposito. Tightening the uncertainty principle for stochastic currents. *Physical Review E*, 94(5):052104, 2016. DOI: [10.1103/PhysRevE.94.052104](https://doi.org/10.1103/PhysRevE.94.052104). URL <https://doi.org/10.1103/PhysRevE.94.052104>.
- [5] André M Timpanaro, Giacomo Guarnieri, John Goold, and Gabriel T Landi. Thermodynamic uncertainty relations from exchange fluctuation theorems. *Physical review letters*, 123(9):090604, 2019. DOI: [10.1103/PhysRevLett.123.090604](https://doi.org/10.1103/PhysRevLett.123.090604). URL <https://doi.org/10.1103/PhysRevLett.123.090604>.
- [6] Timur Koyuk, Udo Seifert, and Patrick Pietzonka. A generalization of the thermodynamic uncertainty relation to periodically driven systems. *Journal of Physics A: Mathematical and Theoretical*, 52(2):02LT02, 2018. DOI: [10.1088/1751-8121/aaec4](https://doi.org/10.1088/1751-8121/aaec4). URL <https://doi.org/10.1088/1751-8121/aaec4>.
- [7] Andre C Barato and Udo Seifert. Thermodynamic uncertainty relation for biomolecular processes. *Physical review letters*, 114(15):158101, 2015. DOI: [10.1103/PhysRevLett.114.158101](https://doi.org/10.1103/PhysRevLett.114.158101). URL <https://doi.org/10.1103/PhysRevLett.114.158101>.
- [8] Raam Uzdin and Saar Rahav. Global passivity in microscopic thermodynamics. *Physical Review X*, 8(2):021064, 2018. DOI: <https://doi.org/10.1103/PhysRevX.8.021064>. URL [10.1103/PhysRevX.8.021064](https://doi.org/10.1103/PhysRevX.8.021064).
- [9] Raam Uzdin and Saar Rahav. Passivity deformation approach for the thermodynamics of isolated quantum setups. *PRX Quantum*, 2(1):010336, 2021. DOI: [10.1103/PRXQuantum.2.010336](https://doi.org/10.1103/PRXQuantum.2.010336). URL <https://doi.org/10.1103/PRXQuantum.2.010336>.
- [10] Philipp Strasberg and Andreas Winter. First and second law of quantum thermodynamics: A consistent derivation based on a microscopic definition of entropy. *PRX Quantum*, 2(3):030202, 2021. DOI: [10.1103/PRXQuantum.2.030202](https://doi.org/10.1103/PRXQuantum.2.030202). URL <https://doi.org/10.1103/PRXQuantum.2.030202>.
- [11] Manabendra Nath et. al. Bera. Thermodynamics as a consequence of information conservation. *Quantum*, 3:121, 2019. DOI: [10.22331/q-2019-02-14-121](https://doi.org/10.22331/q-2019-02-14-121). URL <https://doi.org/10.22331/q-2019-02-14-121>.
- [12] Andre M Timpanaro, Jader P Santos, and Gabriel T Landi. Landauer’s principle at zero temperature. *Physical Review Letters*, 124(24):240601, 2020. DOI: [10.1103/PhysRevLett.124.240601](https://doi.org/10.1103/PhysRevLett.124.240601). URL <https://doi.org/10.1103/PhysRevLett.124.240601>.
- [13] Christopher Jarzynski. Rare events and the convergence of exponentially averaged work values. *Physical Review E*, 73(4):046105, 2006. DOI: [10.1103/PhysRevE.73.046105](https://doi.org/10.1103/PhysRevE.73.046105). URL <https://doi.org/10.1103/PhysRevE.73.046105>.
- [14] Raam Uzdin. The second law and beyond in microscopic quantum setups. In *Thermodynamics in the Quantum Regime*, pages 681–712. Springer, 2018. DOI: [10.1007/978-3-319-99046-0_28](https://doi.org/10.1007/978-3-319-99046-0_28). URL https://doi.org/10.1007/978-3-319-99046-0_28.
- [15] Ivan Henao, Raam Uzdin, and Nadav Katz. Experimental detection of microscopic environments using thermodynamic observables. *arXiv preprint arXiv:1908.08968*, 2019. DOI: [10.48550/arXiv.1908.08968](https://doi.org/10.48550/arXiv.1908.08968). URL <https://doi.org/10.48550/arXiv.1908.08968>.
- [16] Daiwei Zhu, Sonika Johri, Norbert M Linke, KA Landsman, C Huerta Alderete, Nhung H Nguyen, AY Matsuura, TH Hsieh, and Christopher Monroe. Generation of thermofield double states and critical ground states with a quantum computer. *Proceedings of the National Academy of Sciences*, 117(41):25402–25406, 2020. DOI: [10.1073/pnas.2006337117](https://doi.org/10.1073/pnas.2006337117). URL <https://doi.org/10.1073/pnas.2006337117>.
- [17] Michael A Nielsen. An introduction to majorization and its applications to quantum mechanics. *Lecture Notes, Department of Physics, University of Queensland, Australia*, 2002.
- [18] John A Smolin, Frank Verstraete, and Andreas Winter. Entanglement of assistance and multipartite state distillation. *Physical Review A*, 72(5):052317, 2005. DOI: [10.1103/PhysRevA.72.052317](https://doi.org/10.1103/PhysRevA.72.052317). URL <https://doi.org/10.1103/PhysRevA.72.052317>.
- [19] Asher Peres. Quantum theory: concepts and methods, vol. 57. *Fundamental Theories of Physics*, 2006. DOI: [10.1119/1.17946](https://doi.org/10.1119/1.17946). URL <https://doi.org/10.1119/1.17946>.
- [20] Massimiliano Esposito and Christian Van den Broeck. Second law and landauer principle far from equilibrium. *EPL (Europhysics Letters)*, 95(4):40004, 2011. DOI: [10.1209/0295-5075/95/40004](https://doi.org/10.1209/0295-5075/95/40004). URL <https://doi.org/10.1209/0295-5075/95/40004>.

- [21] IM Bassett. Alternative derivation of the classical second law of thermodynamics. *Physical Review A*, 18(5):2356, 1978. DOI: [10.1103/PhysRevA.18.2356](https://doi.org/10.1103/PhysRevA.18.2356). URL <https://doi.org/10.1103/PhysRevA.18.2356>.
- [22] Norbert M Linke, Dmitri Maslov, Martin Roetteler, Shantanu Debnath, Caroline Figgatt, Kevin A Landsman, Kenneth Wright, and Christopher Monroe. Experimental comparison of two quantum computing architectures. *Proceedings of the National Academy of Sciences*, 114(13):3305–3310, 2017. DOI: [10.1073/pnas.1618020114](https://doi.org/10.1073/pnas.1618020114). URL <https://doi.org/10.1073/pnas.1618020114>.
- [23] Prakash Murali, Norbert Matthias Linke, Margaret Martonosi, Ali Javadi Abhari, Nhung Hong Nguyen, and Cinthia Huerta Alderete. Full-stack, real-system quantum computer studies: Architectural comparisons and design insights. In *2019 ACM/IEEE 46th Annual International Symposium on Computer Architecture (ISCA)*, pages 527–540. IEEE, 2019. DOI: [10.48550/arXiv.1905.11349](https://doi.org/10.48550/arXiv.1905.11349). URL <https://doi.org/10.48550/arXiv.1905.11349>.
- [24] Raam Uzdin. Methods for measuring noise, purity changes, and entanglement entropy in quantum devices and systems. *US Provisional Patent: 63/260501*.
- [25] Raam Uzdin. Methods for measuring noise, purity changes, and entanglement entropy in quantum devices and systems. *arXiv preprint arXiv:2112.00546*, 2021. DOI: [10.48550/arXiv.2112.00546](https://doi.org/10.48550/arXiv.2112.00546). URL <https://doi.org/10.48550/arXiv.2112.00546>.
- [26] Dominic V Else, Bela Bauer, and Chetan Nayak. Floquet time crystals. *Physical review letters*, 117(9):090402, 2016. DOI: [10.1103/PhysRevLett.117.090402](https://doi.org/10.1103/PhysRevLett.117.090402). URL <https://doi.org/10.1103/PhysRevLett.117.090402>.
- [27] Pai Peng, Chao Yin, Xiaoyang Huang, Chandrasekhar Ramanathan, and Paola Cappellaro. Floquet prethermalization in dipolar spin chains. *Nature Physics*, 17(4):444–447, 2021. DOI: [10.1038/s41567-020-01120-z](https://doi.org/10.1038/s41567-020-01120-z). URL <https://doi.org/10.1038/s41567-020-01120-z>.
- [28] Jiehang Zhang, Paul W Hess, A Kyprianidis, Petra Becker, A Lee, J Smith, Gaetano Pagano, I-D Potirniche, Andrew C Potter, Ashvin Vishwanath, et al. Observation of a discrete time crystal. *Nature*, 543(7644):217–220, 2017. DOI: [10.1038/nature21413](https://doi.org/10.1038/nature21413). URL <https://doi.org/10.1038/nature21413>.
- [29] Klaus Mølmer and Anders Sørensen. Multiparticle entanglement of hot trapped ions. *Physical Review Letters*, 82(9):1835, 1999. DOI: [10.1103/PhysRevLett.82.1835](https://doi.org/10.1103/PhysRevLett.82.1835). URL <https://doi.org/10.1103/PhysRevLett.82.1835>.
- [30] Enrique Solano, Ruyne Lima de Matos Filho, and Nicim Zagury. Deterministic bell states and measurement of the motional state of two trapped ions. *Physical Review A*, 59(4):R2539, 1999. DOI: [10.1103/PhysRevA.59.R2539](https://doi.org/10.1103/PhysRevA.59.R2539). URL <https://doi.org/10.1103/PhysRevA.59.R2539>.
- [31] GJ Milburn, S Schneider, and DFV James. Ion trap quantum computing with warm ions. *Fortschritte der Physik: Progress of Physics*, 48(9-11):801–810, 2000. DOI: [10.1002/1521-3978\(200009\)48:9/11<801::AID-PROP801>3.0.CO;2-1](https://doi.org/10.1002/1521-3978(200009)48:9/11<801::AID-PROP801>3.0.CO;2-1). URL [https://doi.org/10.1002/1521-3978\(200009\)48:9/11<801::AID-PROP801>3.0.CO;2-1](https://doi.org/10.1002/1521-3978(200009)48:9/11<801::AID-PROP801>3.0.CO;2-1).
- [32] Shi-Liang Zhu, Christopher Monroe, and L-M Duan. Arbitrary-speed quantum gates within large ion crystals through minimum control of laser beams. *EPL (Europhysics Letters)*, 73(4):485, 2006. DOI: [10.1209/epl/i2005-10424-4](https://doi.org/10.1209/epl/i2005-10424-4).
- [33] Taeyoung Choi, Shantanu Debnath, TA Manning, Caroline Figgatt, Z-X Gong, L-M Duan, and Christopher Monroe. Optimal quantum control of multimode couplings between trapped ion qubits for scalable entanglement. *Physical review letters*, 112(19):190502, 2014. DOI: [10.1103/PhysRevLett.112.190502](https://doi.org/10.1103/PhysRevLett.112.190502). URL <https://doi.org/10.1103/PhysRevLett.112.190502>.